Robust but delayed thalamocortical activation of dendritic-targeting inhibitory interneurons

Zhenjun Tan*, Hang Hu*, Z. Josh Huang†, and Ariel Agmon*‡

*Department of Neurobiology and Anatomy and the Sensory Neuroscience Research Center, West Virginia University, Morgantown, WV 26505; and †Cold Spring Harbor Laboratories, Cold Spring Harbor, NY 11724

Edited by Edward G. Jones, University of California, Davis, CA, and approved December 21, 2007 (received for review November 8, 2007)

GABA-releasing cortical interneurons are crucial for the neural transformations underlying sensory perception, providing "feedforward" inhibition that constrains the temporal window for synaptic integration. To mediate feedforward inhibition, inhibitory interneurons need to fire in response to ascending thalamocortical inputs, and most previous studies concluded that ascending inputs activate mainly or solely proximally targeting, parvalbumin-containing "fast-spiking" interneurons. However, when thalamocortical axons fire at frequencies that are likely to occur during natural exploratory behavior, activation of fast-spiking interneurons is rapidly and strongly depressed, implying the paradoxical conclusion that feedforward inhibition is absent when it is most needed. To address this issue, we took advantage of lines of transgenic mice in which either parvalbumin- or somatostatin-containing interneurons express GFP and recorded the responses of interneurons from both subtypes to thalamocortical stimulation *in vitro*. We report that during thalamocortical activation at behaviorally expected frequencies, fast-spiking interneurons were indeed activated only transiently because of rapid depression of their thalamocortical inputs, but a subset of layer 5 somatostatin-containing interneurons were robustly and persistently activated after a delay, due to the facilitation and temporal summation of their thalamocortical excitatory postsynaptic potentials. Somatostatin-containing interneurons are considered distally targeting. Thus, they are likely to provide delayed dendritic inhibition during exploratory behavior, contributing to the maintenance of a balance between cortical excitation and inhibition while leaving a wide temporal window open for synaptic integration and plasticity in distal dendrites.

barrel cortex | dendrites | neocortex | somatostatin | feedforward inhibition

An animal's survival depends on an accurate neural representation of its environment. In the mammalian neocortex, this representation is constructed from a continuously updated stream of sensory information relayed through thalamocortical axons that terminate in cortical layers 4–6 and directly excite principal cortical cells and, even more strongly, GABAergic inhibitory interneurons, as observed both *in vivo* (1, 2) and *in vitro* (3, 4). This powerful engagement of GABAergic interneurons results in short-latency disynaptic or "feedforward" inhibition that is ubiquitously observed in thalamorecipient layers after sensory stimulation *in vivo* (5–7) or intrathalamic stimulation *in vitro* (8–10). Feedforward inhibition imposes a short, frequency-dependent synaptic integration window on the postsynaptic neuron (9, 11) and is highly effective in preempting spiking in principal neurons (3, 4), thus curtailing the cortical response to all but the most salient stimuli (12). Feedforward inhibition is crucial for the extraction of various features of stimulus space (13, 14) and, therefore, for the construction of an accurate neural representation of the sensory environment.

Inhibitory interneurons in the cerebral cortex fall into numerous classes and subtypes (15). The two largest and best studied subtypes are "fast-spiking," parvalbumin-expressing (FS/PV+) cells, which preferentially target somata and proximal dendrites, and somatostatin-expressing (SOM+) interneurons, which preferentially target distal dendrites (16). With a notable exception (3), most previous studies concluded that FS/PV+ interneurons were the main mediators of feedforward thalamocortical inhibition (17–19). This conclusion, however, has a puzzling corollary. During natural exploratory behavior, rats and mice palpate their environment with their whiskers at frequencies of ≈10 Hz, with occasional shorter bouts of "foveal whisking" at frequencies of 15–25 Hz (20, 21). Such whisking episodes would presumably generate thalamocortical spike trains of even higher frequencies because thalamocortical relay neurons fire at least one spike at the onset of a whisker deflection and also often fire at its offset (22, 23). However, thalamocortical activation of FS/PV+ interneurons is greatly reduced at frequencies of ≥10 Hz, resulting in pronounced depression of somatic feedforward inhibition (9, 11, 24). How then are accurate cortical representations maintained during exploratory behavior when such representations are most needed? Here we suggest a solution to this paradox by showing that thalamocortical excitatory postsynaptic potentials (EPSPs) on SOM+ interneurons undergo strong steady-state facilitation and temporal summation at activation frequencies likely to occur during native exploratory behavior. Thus, SOM+ interneurons would be robustly activated during sensory exploration, substituting dendritic-targeted inhibition for the reduced FS-mediated inhibition at the soma.

Results

Facilitation and Summation of Thalamus-Evoked EPSPs in SOM+ Interneurons. We used transgenic mice of the X94 line, in which GFP is specifically expressed in a subset of SOM+ interneurons (25), to record from layer 5 SOM+ interneurons in thalamocortical slices from the whisker ("barrel") somatosensory cortex. For comparison, we recorded from GFP-expressing FS/PV+ interneurons in layers 4–5 of G42 transgenic mice (26), as well as from non-GFP-expressing FS interneurons in X94 or wild-type mice. Consistent with our previous report (25), layer 5 SOM+ interneurons provided dense axonal innervation to layer 4 barrels, whereas FS/PV+ axons mostly ramified locally (Fig. 1*A*). SOM+ and FS/PV+ interneurons were clearly distinguishable by their intrinsic firing patterns (Fig. 1*B*) and by their active and passive membrane parameters (Fig. 1 *C–F*). Other than a minor difference in the adaptation ratio (AR) (0.69 ± 0.02 vs. 0.84 ± 0.04; $P = 0.02$), non-GFP-expressing and GFP-expressing FS/PV+ cells were statistically indistinguishable (Fig. 1 *C–F*) and were pooled in subsequent analysis. We elicited postsynaptic responses by extracellular stimulation in the ventrobasal thalamus (VB) (Fig. 2*A*). At just-suprathreshold stimulus intensities, FS/PV+ neurons fired reliably in response to the first two to three stimuli in a 20-Hz train, but rarely to later stimuli in the

Author contributions: Z.T. performed research; Z.T., H.H., and A.A. analyzed data; and Z.J.H. and A.A. wrote the paper.

The authors declare no conflict of interest.

This article is a PNAS Direct Submission.

‡To whom correspondence should be addressed. E-mail: aric.agmon@gmail.com.

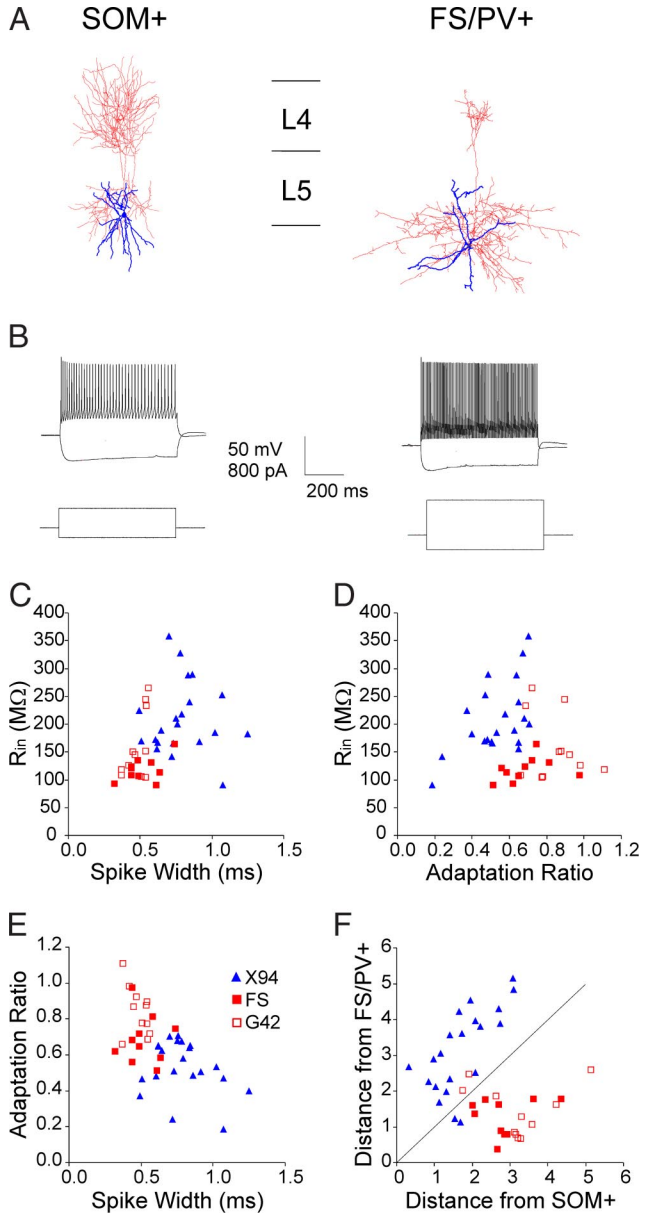

Fig. 1. Morphological and electrophysiological properties of SOM+ versus FS/PV+ interneurons. (*A*) Recorded neurons were filled with biocytin and reconstructed with the Neurolucida system. Cell body and dendrites are represented in blue, axons in red. The SOM+ interneuron had a much more extensive and denser arborization in layer 4. Horizontal lines indicating interlaminar boundaries are 200 μm long. (*B*) Typical sub- and suprathreshold voltage responses (*Upper*) in response to intracellular current injection (*Lower*). (*C–E*) Pairwise scatterplots of input resistance (R_{in}), spike width at half height, and AR. Open red squares represent GFP-expressing FS/PV+ neurons in G42 mice, and filled red squares represent non-GFP-expressing FS cells recorded in X94 or wild-type mice. Note the extensive overlap between these two populations but the clear separation from the SOM+ population (blue triangles). (*F*) Scatterplot of the Mahalanobis distance (a multivariate metric) of each neuron from the centers of the two groups; diagonal line is equidistant from both centers. Note that only two cells from each subtype were closer to the center of the other group than to their own group's center.

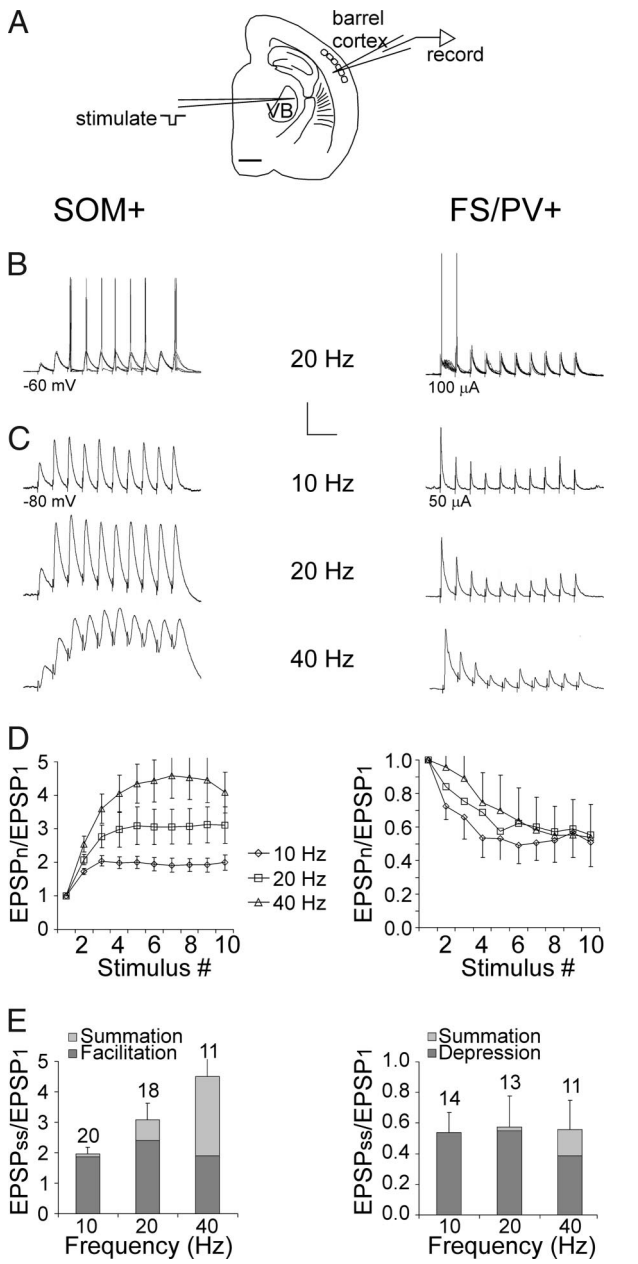

Fig. 2. Dynamics of thalamocortical EPSPs in SOM+ and FS/PV+ interneurons. (*A*) Tracing of a thalamocortical slice indicating typical positions of the stimulating electrode in the VB and of the recording micropipette in the infragranular barrel cortex. (Scale bar: 1 mm.) (*B*) Five superimposed thalamus-evoked responses at 20 Hz. Holding potential (*Left*) and stimulation intensity (*Right*) indicated. (Calibration bar: 25 mV, 100 ms.) (*C*) Averaged subthreshold responses at the indicated frequencies. (Calibration bar: *Top*, 5 mV, 200 ms; *Middle*, 5 mV, 100 ms; *Bottom*, 5 mV, 50 ms.) (*D*) The total depolarization (normalized to the first EPSP) generated by each of 10 stimuli at 10, 20, and 40 Hz. Error bars represent SEM. (*E*) The normalized contributions of facilitation, depression, and temporal summation to the steady-state depolarization in the same dataset as above. Error bars are for the total response. Sample sizes (above bars) apply to *D* as well.

train. In contrast, SOM+ interneurons rarely fired to the first two to three stimuli, but fired reliably afterward (Fig. 2*B*). Similar observations were made in the cell-attached mode, which does not disturb the ionic and biochemical milieu of the cells (data not shown). The basis for these opposite response patterns was revealed when spiking was prevented by hyperpolarization or by reducing the stimulus intensity: EPSPs in 86% of FS/PV+ cells ($n = 14$) underwent strong short-term depression at 10–40 Hz, whereas 90% of SOM+ interneurons ($n = 20$) exhibited short-term facilitation at the same frequencies; ($P = 0.000012$; Fisher's exact test), in addition to pronounced temporal sum-

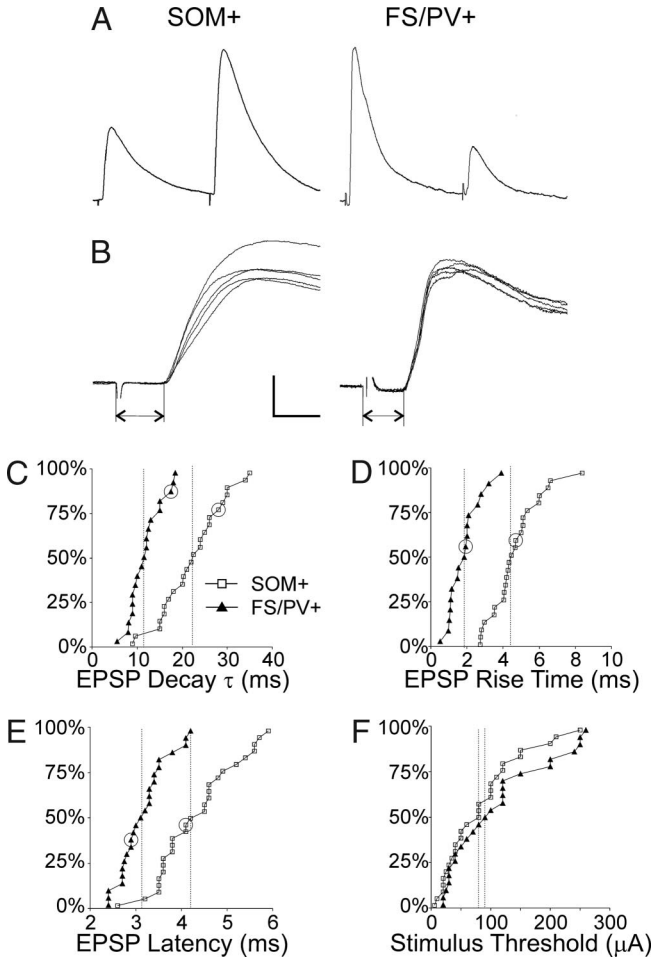

Fig. 3. Properties of thalamocortical EPSPs in SOM+ and FS/PV+ interneurons. (*A*) Representative averaged trace of the first two EPSPs from a 10-Hz train. (*B*) Five superimposed traces from the same cells at a faster time base. Dual arrows indicate synaptic latencies. (Calibration bar: *A*, 4 mV, 40 ms; *B*, 5 mV, 4 ms.) (*C–F*) Cumulative probability histograms comparing EPSP decay τ, rise times, latencies, and thresholds in the two groups of interneurons. Vertical dashed lines indicate the medians in each population. Data points corresponding to the examples in *A* and *B* are circled in *C–E*.

mation at 40 Hz (Fig. 2*C*). The contributions of facilitation, depression, and temporal summation at three different frequencies are summarized in Fig. 2 *D* and *E*. On average, thalamus-evoked EPSPs in FS/PV+ interneurons depressed to about half their initial amplitude during a 10- to 40-Hz train, whereas EPSPs in SOM+ interneurons approximately doubled, with temporal summation at 40 Hz increasing the total steady-state depolarization to more than four times the initial EPSP. Previous studies demonstrated that the same pyramidal cell can mediate low release probability (P_r), facilitating EPSPs in putative SOM+ interneurons, and high P_r, depressing EPSPs in FS/PV+ interneurons (27–29), implying a postsynaptic determination of the release properties of the synapse. Our findings suggest that thalamocortical axons observe the same rules of target-specific short-term dynamics as intracortical ones.

Slower Kinetics and Longer Latencies of Thalamus-Evoked EPSPs in SOM+ Interneurons. The difference in temporal summation between the SOM+ and FS/PV+ groups reflected a difference in the decay time constant of the EPSP (τ_{EPSP}), which was 2-fold slower in SOM+ (22.8 ± 1.4 ms, mean ± SEM, $n = 24$), compared with FS/PV+ cells (11.8 ± 0.84 ms, $n = 19$; $P < 0.00001$, exact permutation test of means, two sided) (Fig. 3 *A* and *C*). The slower EPSP decay in SOM+ interneurons could have simply reflected their higher input resistance (R_{in}) and thereby a longer membrane time constant (τ_m), but our results do not rule out a differential contribution of NMDA receptor-mediated currents (30) or of voltage-dependent conductances (31) to the time course of the EPSPs. In addition, EPSP rise times were on average >2-fold longer in SOM+ interneurons (4.6 ± 0.3 ms, $n = 24$, vs. 1.8 ± 0.2 ms, $n = 17$; $P < 0.00001$) (Fig. 3 *B* and *D*). Latencies of thalamus-evoked EPSPs also were longer in SOM+ interneurons (4.3 ± 0.2 ms, $n = 27$, vs. 3.2 ± 0.1 ms, $n = 25$; $P < 0.00001$) (Fig. 3 *B* and *E*), but the thresholds for evoking EPSPs were not significantly different between the groups ($P = 0.23$) (Fig. 3*F*), implying that the latency differences were not attributable to distinct populations of presynaptic axons differing in diameters and thereby in both thresholds and conduction velocities. More likely, the longer latencies and slower rise times of EPSPs in SOM+ interneurons reflected a slower and less synchronized synaptic release process, possibly reflecting a longer diffusional distance in facilitating synapses between the presynaptic Ca^{2+} channels and the release site (28).

Latencies of Antidromically Evoked Spikes in Corticothalamic Neurons (CTNs). Infragranular pyramidal cells, including putative CTNs, make facilitating synaptic connections on nearby interneurons (32, 33). To rule out that antidromically activated CTN axon collaterals contributed to the facilitating EPSPs in layer 5 SOM+ interneurons, we recorded from infragranular, "regular-spiking" (Fig. 4*A*) pyramidal neurons, in which antidromic spikes could be evoked by intrathalamic stimulation in the same location and at the same range of intensities used for orthodromic stimulation. In all cases ($n = 5$), we verified by a collision test that the spikes were antidromic (Fig. 4*B*). In two cases, we also tested and verified the persistence of the spikes after a pharmacological blockade of EPSPs (Fig. 4*C*), whereas in two other cells, we observed the biocytin-stained axon entering the VB (Fig. 4*D*). Unlike CTNs in the rat (33), CTN axons in our sample did not display supernormality (the change in conduction velocity at 50 Hz ranged from −0.7% to 1.6%). In this subset of CTNs, latencies to antidromic spike onset ranged from 5.7–11.6 ms (median, 6.7 ms). Potential EPSPs evoked by these cells in nearby interneurons would have occurred ≈2 ms later still due to intracortical conduction time and synaptic delay (32). Because thalamus-evoked EPSPs in our sample had latencies of ≤6 ms (Fig. 3*E*), they were highly unlikely to have been mediated by antidromically activated CTNs.

Discussion

SOM+ Interneurons May Be the Main Source of Inhibition During Sensory Exploration. Our results show that FS/PV+ and SOM+ interneurons will respond with different temporal patterns to a train of thalamocortical action potentials. FS/PV+ cells will fire early in the train but transiently, whereas SOM+ interneurons will fire persistently after an initial delay required for the buildup of facilitation and temporal summation of the EPSPs. This implies that much, maybe even most, of the inhibition in thalamo-recipient layers—during sustained thalamocortical activity arising from natural exploratory behavior—will originate from SOM+ rather than FS/PV+ interneurons. SOM+ interneurons preferentially target dendrites (16, 34). Our results, therefore, add to several recent studies in supporting a hitherto little recognized role for dendritic-targeting interneurons in providing a firing rate-dependent control over neocortical and hippocampal excitability (35–37), but are distinct from these previous reports in describing a feedforward, rather than a feedback, mode of activation. Although the ability of dendritic inhibition to control neuronal output is low under quiescent conditions, its efficacy is greatly enhanced during dendritic

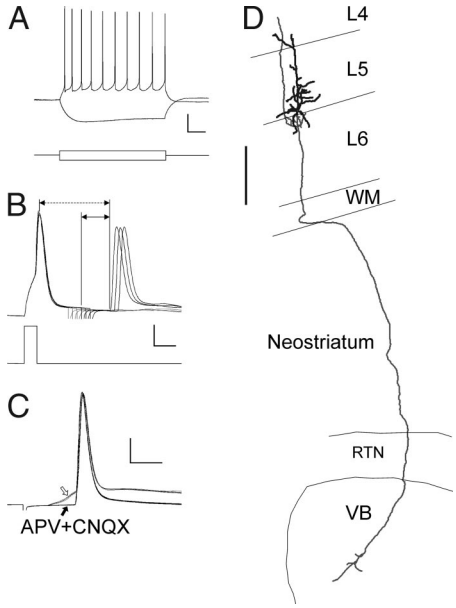

Fig. 4. Antidromic activation of CTNs. (*A*) Typical sub- and suprathreshold voltage responses (*Upper*) of a pyramidal CTN in response to current injection (*Lower*). (Calibration bar: *Upper*, 20 mV, 100 ms; *Lower*, 120 pA, 100 ms.) (*B*) A collision test to verify the antidromic nature of a spike. An action potential (*Upper*) was elicited by an intracellular current injection (*Lower*), followed at increasing latencies (in 1-ms increments, note stimulus artifacts) by intrathalamic stimulation; six traces are superimposed. The first three sweeps (corresponding to the first three stimulus artifacts) failed to elicit an action potential, but the next three stimuli (heavy lines) did. The horizontal dashed line arrow represents the collision interval, and the shorter solid line arrow represents the conduction time (see *Materials and Methods*). (Calibration bar: *Upper*, 20 mV, 5 ms; *Lower*, 350 pA, 5 ms.) (*C*) Pharmacological verification of antidromic spikes. The spike persisted even when the preceding EPSP (hollow arrow) was blocked pharmacologically by APV and CNQX (solid arrow). (Calibration bar: 20 mV, 4 ms.) (*D*) Neurolucida reconstruction of the CTN corresponding to the recording in *A*. Note the apical dendrite terminating in layer 4 and the axon coursing through the white matter (WM), neostriatum, and reticular thalamic nucleus (RTN) and entering the VB, where it arborizes. The main axonal trunk in the VB ended by truncation at the cut surface of the slice. (Scale bar: 250 μm.)

depolarization (38). Active exploratory behavior is expected to generate sustained thalamocortical firing, in turn depolarizing layer 4 dendrites. Thus, SOM+ interneurons seem to be best tuned to precisely those behavioral states in which their efficacy is optimal. In these behavioral states, neocortical SOM+ interneurons are likely to play a pivotal role in maintaining the balance between excitation and inhibition, a role previously attributed exclusively to FS interneurons (39).

Thalamus-Evoked EPSPs Were Not Mediated by Antidromically Activated Corticothalamic Axons. An alternative interpretation of our results is that our intrathalamic stimulation activated axons of CTNs antidromically and that at least some of the EPSPs we observed in SOM+ interneurons were mediated by the intracortical collaterals of these axons. Such antidromically mediated EPSPs would appear monosynaptic, would have longer latencies due to the slower conduction velocities of corticothalamic axons (40, 41), and would undergo facilitation (32, 33). However, FS/PV+ interneurons also receive facilitating EPSPs from CTNs or CTN-like pyramidal cells (32, 33). Thus, the fact that we did not observe EPSPs with similarly long latencies and short-term facilitation in FS/PV+ cells suggests that CTNs were not activated in our experiments. Moreover, compelling evidence against contamination of our results by antidromically mediated EPSPs comes from the direct recording of antidromic spikes in identified CTNs, evoked from the same location and with the same stimulus intensities used to evoke EPSPs. These antidromic spikes had latencies of >5.5 ms. The potential intracortical EPSPs evoked by them would have had latencies of >7.5 ms, which is well beyond the range of EPSP latencies (all ≤6 ms) in our dataset. A previous study of cortically evoked EPSPs in the thalamus (42), performed under identical experimental conditions in terms of species, age, and recording temperature, estimated that corticothalamic EPSP latencies were ≥6 ms, supporting our conclusion.

The Delayed Shift from Somatic to Dendritic Inhibition. Our results imply that a bout of whisking at behaviorally relevant frequencies would evoke transient, FS/PV+-mediated somatic feedforward inhibition, followed ≈50–100 ms later by sustained, SOM+-mediated dendritic inhibition. A similar frequency-dependent, soma-to-dendrites shift in feedback inhibition was previously observed in the hippocampus during high-frequency stimulation *in vitro* (37) and during exploratory behavior *in vivo* (43). What could be the function of such a delayed shift? Distal dendrites form a distinct biophysical compartment with a unique complement of depolarization- and hyperpolarization-activated channels, interacting with synaptic conductances and back-propagating action potentials in complex, nonlinear ways that may enable neuronal information processing and storage (44, 45). These active dendritic processes are tightly controlled by local GABAergic conductances (46, 47). A hallmark of dendritic conductances (e.g., voltage-activated calcium channels or NMDA receptor-mediated currents) is their relatively slow kinetics. Indeed, the processes of synaptic modification, such as spike timing-dependent plasticity, occur over a longer temporal window in distal compared with proximal synapses (48). The delayed arrival of feedforward inhibition in distal dendrites will leave a wider time window open for these slower processes of synaptic integration and plasticity to take effect.

Materials and Methods

Animals. Experimental protocols conformed to the Public Health Service Policy on Humane Care and Use of Laboratory Animals and were approved by the West Virginia University Animal Care and Use Committee. We used 16- to 21-day-old mice (median age: postnatal day 18) from transgenic lines X94 (25) [Tg(Gad1/EGFP)94Agmo/J, stock no. 006334; The Jackson Laboratory] and G42 (26) (from Z.J.H.). By the third postnatal week, feedforward thalamocortical inhibition reached its mature state (19, 24). Transgenic lines were maintained by breeding with wild-type CD-1 mice (Charles River Laboratories), and animals were used as hemizygotes.

Preparation of Thalamocortical Brain Slices. Thalamocortical slices, 450 μm thick, were prepared as described (3, 49) and incubated in artificial cerebrospinal fluid (aCSF) at room temperature for at least 1 h. The aCSF contained 126 mM NaCl, 3 mM KCl, 1.25 mM NaH_2PO_4, 2 mM $CaCl_2$, 1.3 mM $MgSO_4$, 26 mM $NaHCO_3$, and 20 mM D-glucose bubbled with 95% O_2/5% CO_2. For recording, individual slices were transferred to a submersion recording chamber and perfused with room temperature, oxygenated aCSF at a rate of 2–3 ml/min. At room temperature, synaptic latencies were increased ≈2-fold (50, 51), which assisted in separating antidromic from orthodromic responses without affecting the target-specific short-term dynamics of the EPSPs (28).

Electrophysiological Recordings. To record thalamocortical responses, slices were placed with their anterior surface up because intact thalamocortical axons were more likely to be near the anterior surface (52). Patch pipettes (5–7 MΩ resistance) were filled with an intracellular solution of 285–295 mOsm (pH 7.25) containing 122 mM $KMeSO_4$, 10 mM KCl, 2 mM $MgCl_2$, 0.1 mM $CaCl_2$, 1.1 mM EGTA, 10 mM Hepes, 4 mM ATP-Mg, 0.3 mM GTP-Na, and 2 mg/ml biocytin (Sigma–Aldrich). GFP+ neurons were identified under fluorescence illumination and targeted for patch recordings using an Axoclamp 2B amplifier (Molecular Devices). To stimulate thalamocortical axons, a unipolar tungsten microelectrode (AM Systems) was placed in the VB complex or at the border of the VB and the reticular thalamic nucleus (RTN). Then 10- to 40-Hz trains of 10 cathodal current pulses, 0.1 ms each, were delivered every 20 s by using a

Master-8 pulse generator and stimulus isolation unit (AMPI). To determine the EPSP thresholds, stimulus intensities were increased in small increments, from 10 up to a maximum of 300 μA. Recorded signals were filtered at 3 kHz and digitized at 10 kHz with a National Instruments ADC board and were acquired by using custom-made software written in the LabView environment (National Instruments). Reported membrane potentials are positively biased by 8 mV, the measured liquid junction potential with our solutions.

Data Analysis. All cells included in the analysis had resting membrane potentials more negative than -60 mV and spike amplitudes (from threshold to peak) of at least 45 mV. EPSPs with latencies >6 ms ($n = 3$) were considered of ambiguous origin and were eliminated from the analysis. To quantify facilitation and depression, several (typically 10) responses to the same stimulation frequency and intensity were averaged, and EPSP amplitudes (from just before response onset to peak) were normalized by the amplitude of the first EPSP in the train. To quantify summation, the residual depolarization from resting membrane potential to just before response onset was normalized by the amplitude of the first EPSP. Thus, the first EPSP in the train had a facilitation value of 1 and a summation value of 0. Steady-state values of facilitation, depression, and summation were defined as the average values for the last four responses in the train. EPSP latencies were measured as shown in Fig. 3*B* (double arrows), from the beginning of the stimulus artifact to the beginning of the voltage deflection. The AR was defined as the ratio of the first interspike interval (ISI) to the average of the last four ISIs at the maximal current step applied before spike inactivation became evident. Spike width was measured at half height between threshold and peak. EPSP decay time constant (τ_{EPSP}) was determined from the monoexponential curve best fitting the falling phase of the EPSP. Fitting was done by using the Levenberg–Marquardt algorithm as implemented in LabView. The EPSP rise time was measured between 10% and 90% of the peak amplitude.

Antidromic Spikes in CTNs. To record antidromic spikes, slices were placed with their posterior surface up because CTNs with intact axons are more likely to be found near the posterior surface (52). The stimulating electrode was placed at the border of the VB and RTN, as before. To differentiate antidromic from orthodromic spikes, some slices were perfused with the NMDA receptor antagonist D-2-amino-5-phosphopentanoic acid (ADV 20 μM; Sigma–RBI) and the AMPA/kainate receptor antagonist 6-cyano-7-nitroquinoxaline-2,3-dione (CNQX, 20 μM; Sigma–RBI) to block excitatory neurotransmission. Spike collision was tested by eliciting an orthodromically propagating spike intracellularly, followed at increasing intervals by an antidromically propagating spike elicited extracellularly. The ''collision interval'' was defined as the interval between the orthodromic spike and the earliest occurring antidromic spike (Fig. 4*B*, dashed line arrow), which should equal twice the antidromic conduction time plus the refractory period (53). Therefore, to be considered antidromic, a spike needed to fulfill the inequality: collision interval larger than two times the conduction time. We included in the analysis only antidromic spikes evoked by stimulation intensities $\leq$300 μA, the same range used for evoking EPSPs. Stronger stimulation intensities (up to 750 μA) could in some cells elicit antidromic spikes at shorter latencies. However, at these higher current levels, it was impossible to rule out current spread to the nearby internal capsule and activation of non-CTN corticofugal axons, which are known to have much faster conduction velocities (40).

Morphological Reconstruction of Recorded Neurons. For morphological reconstruction, slices were fixed overnight in 4% paraformaldehyde in 0.1 M PBS and processed for diaminobenzidine reaction as described (25). Biocytin-filled neurons were then reconstructed digitally by using the Neurolucida system (Microbrightfield) under a $\times$60 water-immersion objective (Olympus) with a working distance of $\approx$130 μm.

Statistics and Multivariate Analysis. All data are reported as mean $\pm$ SEM unless noted otherwise, and all statistical tests were of difference between means unless noted otherwise. Exact two-tailed *P* values were computed by conducting 100,000 random permutations of the dataset and counting the frequency of values as or more extreme than the experimental results (54). Computations were done in MathCad (MathSoft). Mahalanobis distances (55) were calculated in Statistica (StatSoft) from three variables for each cell (R_{in}, spike width, and AR).

ACKNOWLEDGMENTS. We thank Drs. Liset M. de la Prida and Yael Amitai, and members of the West Virginia University Sensory Neuroscience Research Center for comments on previous versions of this manuscript, and Cary Johnson and Angela Harrison for excellent technical and administrative support. This work was supported by National Institutes of Health Grants NS050437 (to A.A.) and RR15574 (to the West Virginia University Sensory Neuroscience Research Center).

1. Swadlow HA (1995) Influence of VPM afferents on putative inhibitory interneurons in S1 of the awake rabbit: Evidence from cross-correlation, microstimulation, and latencies to peripheral sensory stimulation. *J Neurophysiol* 73:1584–1599.
2. Bruno RM, Simons DJ (2002) Feedforward mechanisms of excitatory and inhibitory cortical receptive fields. *J Neurosci* 22:10966–10975.
3. Porter JT, Johnson CK, Agmon A (2001) Diverse types of interneurons generate thalamus-evoked feedforward inhibition in the mouse barrel cortex. *J Neurosci* 21:2699–2710.
4. Cruikshank SJ, Lewis TJ, Connors BW (2007) Synaptic basis for intense thalamocortical activation of feedforward inhibitory cells in neocortex. *Nat Neurosci* 10:462–468.
5. Wilent WB, Contreras D (2004) Synaptic responses to whisker deflections in rat barrel cortex as a function of cortical layer and stimulus intensity. *J Neurosci* 24:3985–3998.
6. Ferster D, Jagadeesh B (1992) EPSP-IPSP interactions in cat visual cortex studied with in vivo whole-cell patch recording. *J Neurosci* 12:1262–1274.
7. Wehr M, Zador AM (2003) Balanced inhibition underlies tuning and sharpens spike timing in auditory cortex. *Nature* 426:442–446.
8. Agmon A, Connors BW (1992) Correlation between intrinsic firing patterns and thalamocortical synaptic responses of neurons in mouse barrel cortex. *J Neurosci* 12:319–329.
9. Gabernet L, Jadhav SP, Feldman DE, Carandini M, Scanziani M (2005) Somatosensory integration controlled by dynamic thalamocortical feedforward inhibition. *Neuron* 48:315–327.
10. Gil Z, Amitai Y (1996) Properties of convergent thalamocortical and intracortical synaptic potentials in single neurons of neocortex. *J Neurosci* 16:6567–6578.
11. Higley MJ, Contreras D (2006) Balanced excitation and inhibition determine spike timing during frequency adaptation. *J Neurosci* 26:448–457.
12. Swadlow HA (2003) Fast-spike interneurons and feedforward inhibition in awake sensory neocortex. *Cereb Cortex* 13:25–32.
13. Wilent WB, Contreras D (2005) Dynamics of excitation and inhibition underlying stimulus selectivity in rat somatosensory cortex. *Nat Neurosci* 8:1364–1370.
14. Miller KD, Pinto DJ, Simons DJ (2001) Processing in layer 4 of the neocortical circuit: New insights from visual and somatosensory cortex. *Curr Opin Neurobiol* 11:488–497.
15. Kawaguchi Y, Kondo S (2002) Parvalbumin, somatostatin and cholecystokinin as chemical markers for specific GABAergic interneuron types in the rat frontal cortex. *J Neurocytol* 31:277–287.
16. Di Cristo G, *et al*. (2004) Subcellular domain-restricted GABAergic innervation in primary visual cortex in the absence of sensory and thalamic inputs. *Nat Neurosci* 7:1184–1186.
17. Sun QQ, Huguenard JR, Prince DA (2006) Barrel cortex microcircuits: Thalamocortical feedforward inhibition in spiny stellate cells is mediated by a small number of fast-spiking interneurons. *J Neurosci* 26:1219–1230.
18. Gibson JR, Beierlein M, Connors BW (1999) Two networks of electrically coupled inhibitory neurons in neocortex. *Nature* 402:75–79.
19. Daw MI, Ashby MC, Isaac JT (2007) Coordinated developmental recruitment of latent fast spiking interneurons in layer IV barrel cortex. *Nat Neurosci* 10:453–461.
20. Carvell GE, Simons DJ (1990) Biometric analyses of vibrissal tactile discrimination in the rat. *J Neurosci* 10:2638–2648.
21. Berg RW, Kleinfeld D (2003) Rhythmic whisking by rat: Retraction as well as protraction of the vibrissae is under active muscular control. *J Neurophysiol* 89:104–117.
22. Armstrong-James M, Callahan CA (1991) Thalamo-cortical processing of vibrissal information in the rat: II. Spatiotemporal convergence in the thalamic ventroposterior medial nucleus (VPm) and its relevance to generation of receptive fields of S1 cortical ''barrel'' neurones. *J Comp Neurol* 303:211–224.
23. Hartings JA, Temereanca S, Simons DJ (2003) Processing of periodic whisker deflections by neurons in the ventroposterior medial and thalamic reticular nuclei. *J Neurophysiol* 90:3087–3094.
24. Agmon A, O'Dowd DK (1992) NMDA receptor-mediated currents are prominent in the thalamocortical synaptic response before maturation of inhibition. *J Neurophysiol* 68:345–349.
25. Ma Y, Hu H, Berrebi AS, Mathers PH, Agmon A (2006) Distinct subtypes of somatostatin-containing neocortical interneurons revealed in transgenic mice. *J Neurosci* 26:5069–5082.
26. Chattopadhyaya B, *et al*. (2004) Experience and activity-dependent maturation of perisomatic GABAergic innervation in primary visual cortex during a postnatal critical period. *J Neurosci* 24:9598–9611.
27. Reyes A, *et al*. (1998) Target-cell-specific facilitation and depression in neocortical circuits. *Nat Neurosci* 1:279–285.
28. Rozov A, Burnashev N, Sakmann B, Neher E (2001) Transmitter release modulation by intracellular Ca2+ buffers in facilitating and depressing nerve terminals of pyramidal cells in layer 2/3 of the rat neocortex indicates a target cell-specific difference in presynaptic calcium dynamics. *J Physiol* 531:807–826.
29. Koester HJ, Johnston D (2005) Target cell-dependent normalization of transmitter release at neocortical synapses. *Science* 308:863–866.
30. Maccaferri G, Dingledine R (2002) Control of feedforward dendritic inhibition by NMDA receptor-dependent spike timing in hippocampal interneurons. *J Neurosci* 22:5462–5472.

31. Thomson AM, Girdlestone D, West DC (1988) Voltage-dependent currents prolong single-axon postsynaptic potentials in layer III pyramidal neurons in rat neocortical slices. *J Neurophysiol* 60:1896–1907.
32. West DC, Mercer A, Kirchhecker S, Morris OT, Thomson AM (2006) Layer 6 cortico-thalamic pyramidal cells preferentially innervate interneurons and generate facilitating EPSPs. *Cereb Cortex* 16:200–211.
33. Beierlein M, Connors BW (2002) Short-term dynamics of thalamocortical and intracortical synapses onto layer 6 neurons in neocortex. *J Neurophysiol* 88:1924–1932.
34. Leranth C, Malcolm AJ, Frotscher M (1990) Afferent and efferent synaptic connections of somatostatin-immunoreactive neurons in the rat fascia dentata. *J Comp Neurol* 295:111–122.
35. Silberberg G, Markram H (2007) Disynaptic inhibition between neocortical pyramidal cells mediated by Martinotti cells. *Neuron* 53:735–746.
36. Kapfer C, Glickfeld LL, Atallah BV, Scanziani M (2007) Supralinear increase of recurrent inhibition during sparse activity in the somatosensory cortex. *Nat Neurosci* 10:743–753.
37. Pouille F, Scanziani M (2004) Routing of spike series by dynamic circuits in the hippocampus. *Nature* 429:717–723.
38. Williams SR, Stuart GJ (2003) Voltage- and site-dependent control of the somatic impact of dendritic IPSPs. *J Neurosci* 23:7358–7367.
39. Shu Y, Hasenstaub A, McCormick DA (2003) Turning on and off recurrent balanced cortical activity. *Nature* 423:288–293.
40. Swadlow HA, Weyand TG (1981) Efferent systems of the rabbit visual cortex: Laminar distribution of the cells of origin, axonal conduction velocities, and identification of axonal branches. *J Comp Neurol* 203:799–822.
41. Ferster D, Lindstrom S (1985) Synaptic excitation of neurones in area 17 of the cat by intracortical axon collaterals of cortico-geniculate cells. *J Physiol* 367:233–252.
42. Golshani P, Liu XB, Jones EG (2001) Differences in quantal amplitude reflect GluR4-subunit number at corticothalamic synapses on two populations of thalamic neurons. *Proc Natl Acad Sci USA* 98:4172–4177.
43. Moser EI (1996) Altered inhibition of dentate granule cells during spatial learning in an exploration task. *J Neurosci* 16:1247–1259.
44. Poirazi P, Mel BW (2001) Impact of active dendrites and structural plasticity on the memory capacity of neural tissue. *Neuron* 29:779–796.
45. Magee JC, Johnston D (2005) Plasticity of dendritic function. *Curr Opin Neurobiol* 15:334–342.
46. Perez-Garci E, Gassmann M, Bettler B, Larkum ME (2006) The GABAB1b isoform mediates long-lasting inhibition of dendritic Ca2+ spikes in layer 5 somatosensory pyramidal neurons. *Neuron* 50:603–616.
47. Kim HG, Beierlein M, Connors BW (1995) Inhibitory control of excitable dendrites in neocortex. *J Neurophysiol* 74:1810–1814.
48. Froemke RC, Poo MM, Dan Y (2005) Spike-timing-dependent synaptic plasticity depends on dendritic location. *Nature* 434:221–225.
49. Agmon A, Connors BW (1991) Thalamocortical responses of mouse somatosensory (barrel) cortex in vitro. *Neuroscience* 41:365–379.
50. Silver RA, Cull-Candy SG, Takahashi T (1996) Non-NMDA glutamate receptor occupancy and open probability at a rat cerebellar synapse with single and multiple release sites. *J Physiol* 494:231–250.
51. Berg-Johnsen J, Langmoen IA (1992) Temperature sensitivity of thin unmyelinated fibers in rat hippocampal cortex. *Brain Res* 576:319–321.
52. Agmon A, Yang LT, O'Dowd DK, Jones EG (1993) Organized growth of thalamocortical axons from the deep tier of terminations into layer IV of developing mouse barrel cortex. *J Neurosci* 13:5365–5382.
53. Fuller JH, Schlag JD (1976) Determination of antidromic excitation by the collision test: Problems of interpretation. *Brain Res* 112:283–298.
54. Good PI (1999) *Resampling Methods* (Birkhauser, Boston).
55. Manly BFJ (2005) *Multivariate Statistical Methods: A Primer* (Chapman & Hall/CRC, Boca Raton, FL).